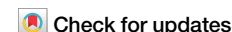


<https://doi.org/10.1038/s41612-025-01097-7>

# Source apportionment of PM<sub>10</sub> based on offline chemical speciation data at 24 European sites



Xiansheng Liu<sup>1,2,3</sup>, Xun Zhang<sup>4,5,6</sup>✉, Bowen Jin<sup>4,5</sup>, Tao Wang<sup>7</sup>✉, Siyuan Qian<sup>4,5</sup>, Jin Zou<sup>6</sup>, Vy Ngoc Thuy Dinh<sup>8</sup>, Jean-Luc Jaffrezo<sup>8</sup>, Gaëlle Uzu<sup>8</sup>, Pamela Dominutti<sup>8</sup>, Sophie Darfeuil<sup>8</sup>, Olivier Favez<sup>9,10</sup>, Sébastien Conil<sup>11</sup>, Nicolas Marchand<sup>12</sup>, Sonia Castillo<sup>13,14</sup>, Jesús D. de la Rosa<sup>15</sup>, Stuart Grange<sup>16</sup>, Christoph Hueglin<sup>16</sup>, Konstantinos Eleftheriadis<sup>17</sup>, Evangelia Diapouli<sup>17</sup>, Manousos-Ioannis Manousakas<sup>17</sup>, Maria Gini<sup>17</sup>, Silvia Nava<sup>18</sup>, Giulia Calzolari<sup>18</sup>, Célia Alves<sup>19</sup>, Marta Monge<sup>3</sup>, Cristina Reche<sup>3</sup>, Roy M. Harrison<sup>20</sup>, Philip K. Hopke<sup>21,22</sup>, Andrés Alastuey<sup>3</sup> & Xavier Querol<sup>3</sup>

This study applied Positive Matrix Factorization (PMF) to PM<sub>10</sub> speciation datasets from 24 urban sites across six European countries (France, Greece, Italy, Portugal, Spain, and Switzerland) to perform a detailed source apportionment (SA) analysis. By using a consistent source apportionment tool for all datasets, the study enhances the comparability of PM<sub>10</sub> SA results across urban Europe. The results identified seven major PM<sub>10</sub> sources including road traffic, biomass burning, crustal/mineral sources, secondary aerosols, industrial emissions, sea salt, and heavy oil combustion (HOC). Road traffic emerged as the predominant source of PM<sub>10</sub> in urban areas, with contributions varying by location, but representing as much as 41% in high-traffic zones. Biomass burning was detected at 23 sites, contributing 8% to 41% on yearly averages, with substantial increase in winter. Crustal sources were present at all sites (3–33%). Industrial sources contributed relatively less PM<sub>10</sub> mass, which was identified at 10 sites with contributions ranging from 2% to 14%. Secondary inorganic and organic aerosol, consisting primarily of ammonium nitrates and sulfates, and organic matter, formed a portion of the PM<sub>10</sub> mass (5–41%). These secondary factors are primarily influenced by anthropogenic emissions, including the various combustion processes. Sea salt, predominantly found in coastal areas, contributed between 4% and 21%, reflecting the impact of the marine environments on air quality. This source was very often ‘aged’ (mixed with anthropogenic pollutants from different origins). Additionally, HOC, especially emits from shipping activities, and traced by V and Ni, was also a frequent contributing source (2–15% for 9 sites), indicating a need for more stringent emission controls. The chemical comparison is performed which indicates road traffic and secondary aerosols, showed consistent chemical profiles across sites, while industrial, HOC, and crustal sources displayed significant site-specific variability. These findings underscore the need for tailored air quality strategies according to local sources of emissions and the importance of long-term PM speciation monitoring for effective pollution control.

Particulate matter (PM) is a complex and harmful atmospheric pollutant<sup>1–3</sup>. The toxicity of PM is determined by its physicochemical properties, including size, shape, and composition, which affect deposition in different regions of the respiratory tract and subsequent biological responses<sup>4</sup>. Particle behavior in the atmosphere and respiratory system largely depends on

these properties, especially size. The size range of particles extends from nanometers to tens of micrometers, which also influences their behavior in the respiratory system. PM<sub>10</sub> encompasses all ambient particulate matter with an aerodynamic diameter less than or equal to 10 µm. Particles in these size ranges can penetrate the initial defenses of the nose, throat, penetrate the

A full list of affiliations appears at the end of the paper. ✉e-mail: [zhangxun@btbu.edu.cn](mailto:zhangxun@btbu.edu.cn); [wangtao\\_fd@fudan.edu.cn](mailto:wangtao_fd@fudan.edu.cn)

larynx, and deposit along the thoracic airways. Therefore, the World Health Organization (WHO)'s 2021 air quality guidelines proposed a 24-h average concentration limit for PM<sub>10</sub> at 45 µg/m<sup>3</sup>, while the European Union (EU) has adopted the same daily limit in latest European AQ Directive (2024/2881/EC)<sup>5</sup>, allowing no more than 18 exceedances per calendar year.

Despite significant improvements in air quality across the EU over the past three decades<sup>6</sup>, air pollution remains the leading environmental factor contributing to premature mortality<sup>1,7,8</sup>. In a recent study, we analyzed the spatiotemporal distribution of 20 trace elements at 55 monitoring sites across Europe from 2013 to 2022<sup>9</sup>, revealing that these trace element concentrations have decreased substantially compared to a decade ago (2006–2015). Unfortunately, concentrations of PM<sub>10</sub> have not fallen at the same rate, and health risks are still substantial in many types of environments<sup>9</sup>. This underscores the need for source apportionment studies to identify PM<sub>10</sub> sources and implement targeted control measures, particularly given the variability in pollutant composition and trends across sites, suggesting diverse origins<sup>9,10</sup>.

Globally, extensive PM<sub>10</sub> source apportionment has been conducted. Reviews by Viana et al.<sup>11</sup> and Hopke et al.<sup>12</sup>, among others, have identified road traffic, biomass burning, heavy oil combustion (HOC), mineral matter, sea salt, and industrial emissions as major sources contributing to urban PM concentrations. Additionally, a substantial portion of PM, if not the largest, is attributed to secondary inorganic and organic aerosols (SIA and SOA, respectively). These studies have informed regional air quality management; however, most European research on assessment of PM sources has been limited to short-term analyses at individual sites<sup>13–17</sup>, even if some synthesis exist for France<sup>18</sup> and Switzerland<sup>19</sup>. This highlights the need for long-term, transnational, and multi-site studies over Europe to better understand PM<sub>10</sub> sources and develop effective strategies to protect urban populations' health.

However, the scarcity of long-term PM<sub>10</sub> speciation data in urban Europe poses a challenge for effective source apportionment. RI-URBANS (Research Infrastructures Services Reinforcing Air Quality Monitoring Capacities in European Urban & Industrial Areas, funded by the European Union's Horizon 2020 research and innovation program, 101036245) aims to develop and apply advanced air quality tools that complement existing air quality monitoring networks (AQMN). In this study, the tool is applied through detailed PM<sub>10</sub> chemical characterization and source apportionment using receptor modeling, contributing to improved understanding of pollution sources and their health implications in urban environments. The present study focuses on the collection and evaluation of data from 24 urban monitoring stations with extensive measurements of chemical tracers located across six European countries (France, Greece, Italy, Portugal, Spain and Switzerland). To identify PM sources, Positive Matrix Factorization (PMF) was applied individually at each site due to its capability to handle complex datasets and resolve multiple sources without requiring prior information about the sources<sup>12,18,20–23</sup>. This standardized approach enables a more comprehensive understanding of air pollution patterns in Europe, ultimately facilitating the formulation of effective strategies to improve air quality in European cities.

## Results and discussion

### Overview across monitoring sites of the concentrations used for the inputs of the PMF studies

The study compared the concentration variations of 32 detected metrics across all sites and different types of monitoring sites (UB, TR, IND, SUB) (Fig. 1 and Supplementary Fig. 1). To assess whether the distributions of PM<sub>10</sub> component concentrations conformed to normality assumptions, we applied the Kolmogorov–Smirnov test. The results showed that most species exhibited non-normal distributions across sites, and thus non-parametric methods were used for subsequent statistical comparisons. Subsequently, Dunn's post hoc test<sup>24</sup> was conducted to compare differences in the same metrics among paired monitoring site types. The results of the overall Kruskal–Wallis test<sup>25</sup> indicated significant differences among monitoring sites for most species, except for Na, Mg, K, Ca, Cr, Rb, Cd, Sn, Sb, and Cl<sup>−</sup> (see Supplementary Table 1). Figure 1 illustrates that the main components

in the PM<sub>10</sub> at all sites are OC, EC, Fe, Al, Na, Mg, K, Ca, and inorganic ions (NH<sub>4</sub><sup>+</sup>, Cl<sup>−</sup>, NO<sub>3</sub><sup>−</sup>, and SO<sub>4</sub><sup>2−</sup>). For a detailed description of these chemical speciation concentration ranges at different site types, refer to the Supplementary section 1 and Liu et al.<sup>9</sup>.

In addition, Pearson correlation analysis was conducted on the species-to-PM<sub>10</sub> ratios across different locations (see Supplementary Fig. 2). Using ratios rather than absolute concentrations helps minimize the influence of mass loading variability across sites and emphasizes the compositional similarities that are more indicative of common emission sources. This analysis revealed robust positive correlations among certain relative abundances, suggesting shared geochemical characteristics or common sources<sup>9,26</sup>. For a more detailed discussion of overall correlations, seasonal variations, and different types of monitoring sites in metrics (UB, TR, IND, SUB), refer to our previous study<sup>9</sup>, which also demonstrated that specific indicators serve as reliable markers for source apportionment. Meanwhile, the study also found that all concentrations showed significant differences across the various monitoring sites (Fig. 1), with industrial and traffic areas tending to have higher concentrations of most indicators, reflecting the greater impact of industrial and traffic-related pollution<sup>27,28</sup>. For instance, at TR sites, components such as OC, EC, Cr, Cu, Zn, As, Rb, Sn, Sb, and Ba showed elevated levels. This is primarily because traffic sites are exposed to high vehicular emissions, brake wear, and tire wear, which contribute significantly to the levels of these elements<sup>28,29</sup>. In contrast, at UB sites, elements such as Na or Na<sup>+</sup>, Mg or Mg<sup>2+</sup>, Al, Cl<sup>−</sup>, K, Ca or Ca<sup>2+</sup>, Ti, V, Mn, Fe, Ni, Cd, and Pb were more prominent. The higher levels of these elements in UB areas can be attributed to a combination of sources, including resuspended road dust, domestic activity, industrial emissions transported over longer distances, and natural sources such as sea spray and soil dust<sup>30,31</sup>.

With respect to SIA, DEM\_SUB particularly, located 10 km north-east of downtown Athens at an altitude of 280 m a.s.l, surrounded by Mediterranean vegetation (mainly pine trees), displayed notably higher concentrations of secondary inorganic ions NH<sub>4</sub><sup>+</sup> and SO<sub>4</sub><sup>2−</sup> in agreement with results from Eleftheriadis et al.<sup>32</sup> and Vasilatou et al.<sup>33</sup>. It suggests the significant impact of photochemical transformation and regional transport of precursors such as NH<sub>3</sub> and SO<sub>2</sub> to this region. However, it's important to recognize that these conditions may not fully represent general suburban conditions across Europe.

### PM<sub>10</sub> source apportionments

As shown in Fig. 2, solutions with 5–9 factors provided the most suitable and reliable outcomes across the 24 monitoring sites, based on the stability of factor profiles and their alignment with known pollution sources<sup>11,12,34</sup>. In summary, sources of ambient PM<sub>10</sub> have been grouped into 7 categories: road traffic (including exhaust and non-exhaust vehicle emissions), biomass burning, a crustal source, a SIA + SOA, industrial source, sea-salt source, a mixed fuel-oil combustion (with or without shipping), and other specific sources. The identification of each source was based on the presence and relative contributions of well-established chemical markers, as summarized in Supplementary Table 2. These solutions illustrate the contributions of various pollution sources to PM<sub>10</sub> concentrations, with road traffic, biomass burning, crustal, and secondary sulfate sources being the most common (identified at 22–24 sites). By contrast, industrial and sea-salt sources were less frequently identified, reflecting their more localized or episodic contributions. Meanwhile, the source profiles identified by the PMF analysis are shown in Supplementary Fig. 3 and the temporal series of each source contribution to PM<sub>10</sub> are displayed in Supplementary Fig. 4. By comparing PM<sub>10</sub> contributions across sites, differences in source contributions are evident for urban, suburban, and industrial areas. A notable limitation in this study is the inconsistent inclusion of key tracers across sites. For example, levoglucosan, an important marker for biomass burning, was only available at 9 of the 24 monitoring sites. Sensitivity analyses at these nine sites revealed that biomass burning could still be identified at eight sites even in the absence of levoglucosan, with comparable contribution estimates (see Supplementary Fig. 5). However, at one site (ZUR\_UB), the biomass burning factor could not be resolved without levoglucosan. This suggests that while levoglucosan

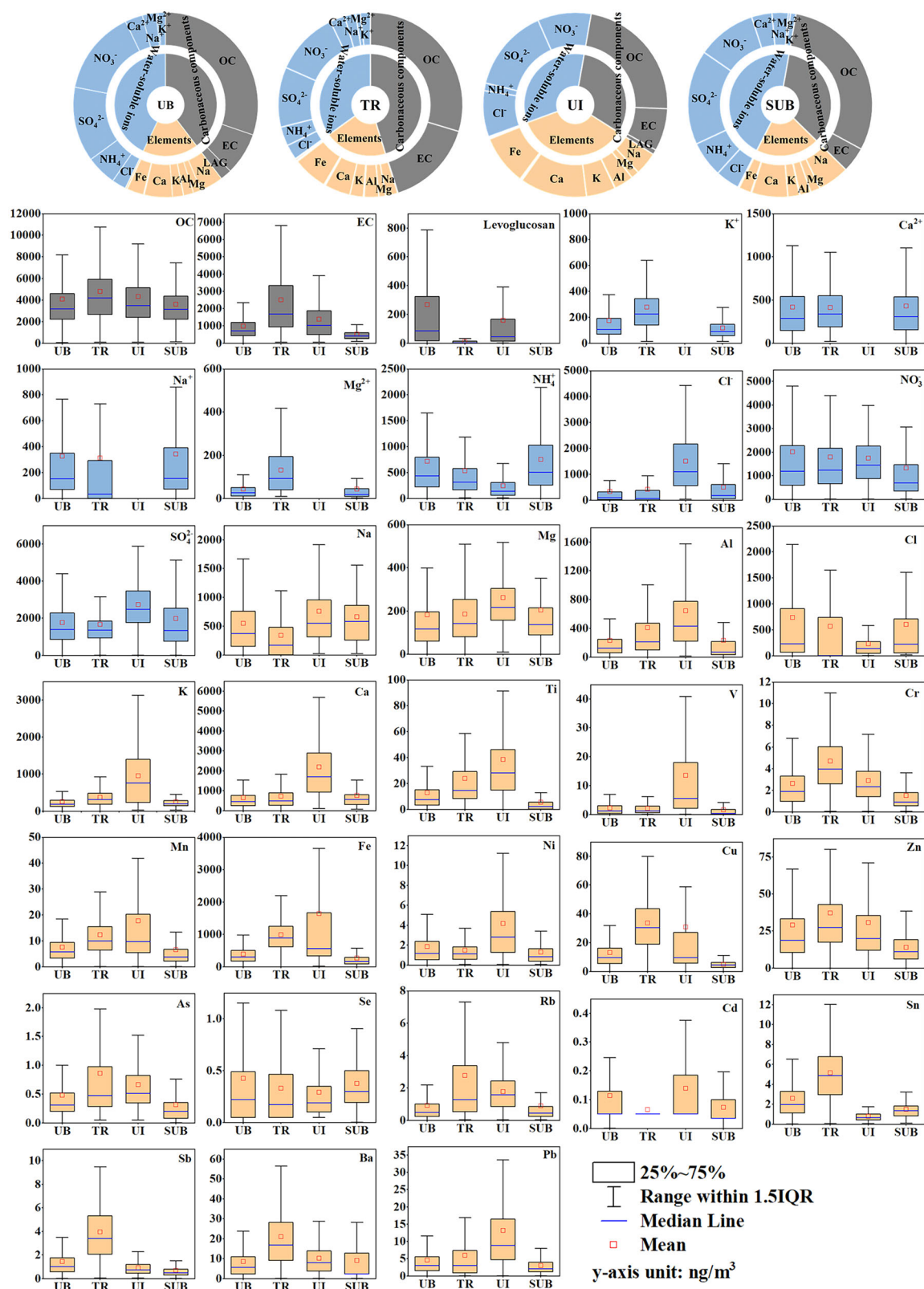


**Fig. 1** | The concentrations of metrics at different types monitoring sites (UB urban background, TR traffic, UI urban industry, SUB suburban).

enhances source resolution and quantification, its absence does not inevitably lead to source misclassification, although it may increase uncertainty. These findings highlight the need for harmonized chemical speciation protocols in multi-site studies to ensure reliable and comparable source apportionment, especially for sources with overlapping chemical profiles.

### Overall comparison of source contributions: profiles and temporal variability

The similarities among all the chemical profiles identified in this study were first analyzed using tools developed within the framework of FAIRMODE (Forum for Air Quality Modeling) activities, as presented by Belis et al.<sup>35</sup>,

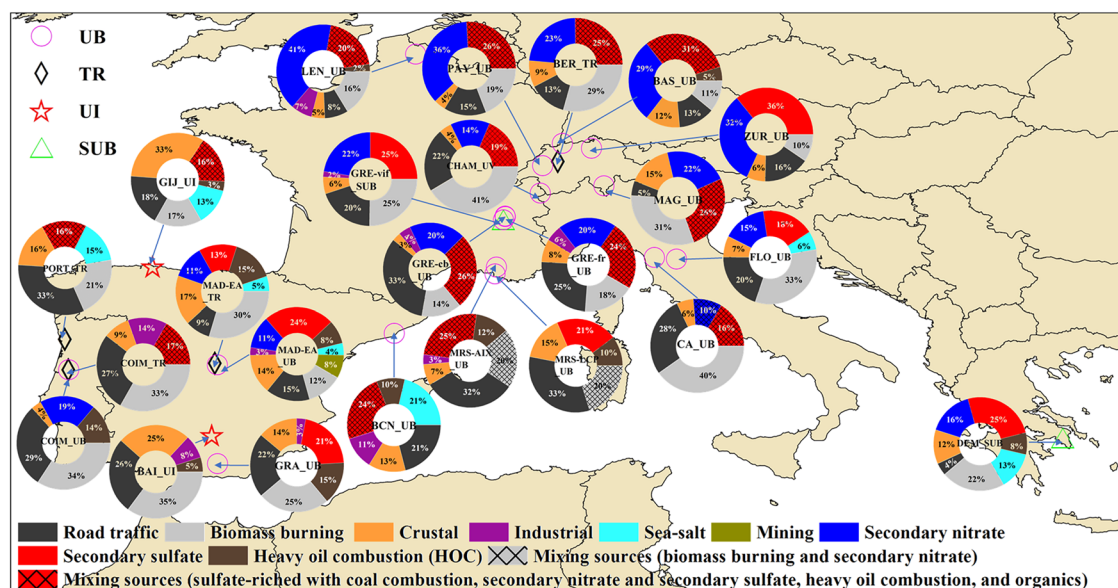
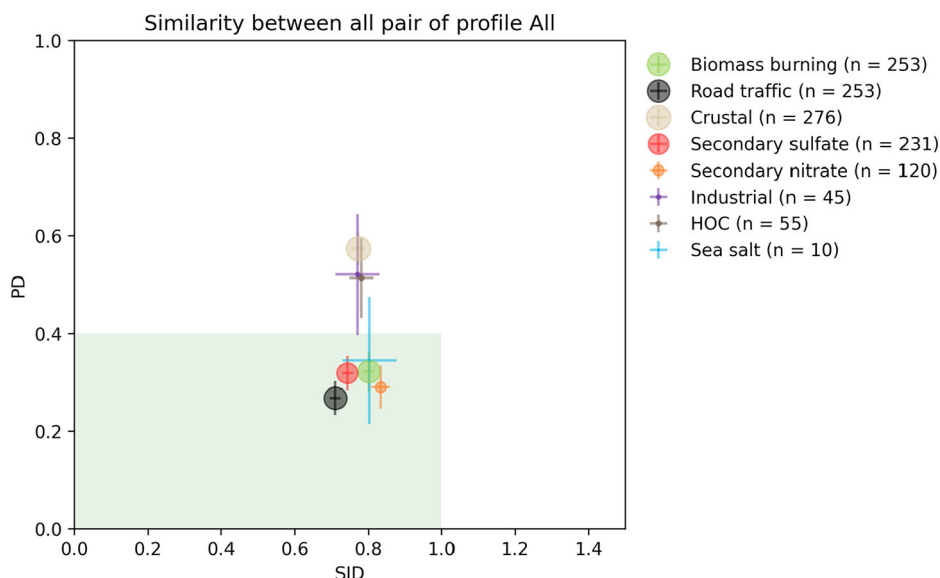


**Fig. 2** | Quantitative source apportionment (with PMF) of mean PM<sub>10</sub> concentrations for 24 locations across 6 countries in Europe.

**Fig. 3** | Similarity plot for all chemical profile in 24 sites of profiles belonging to the same factor/source category in this study. The mean  $\pm$  standard deviation for a given source category is plotted. The size of the dot is proportional to the number of available pair of profile (from 10 to 276, shown in parenthesis in the legend). The green box highlights the acceptable area for profile similarity according to Pernigotti and Belis<sup>118</sup>.



based on the relative chemical profile of runs under a unified protocol. PMF factor profiles attributed to specific source categories were compared using two similarity indicators: PD (Pearson Distance) and SID (Standardized Identity Distance). Factors identified at certain sites were excluded from this analysis when they exhibited significant mixing with other emission sources, making them less representative of a distinct source category. The SID and PD analysis was performed after the pollution sources were resolved using PMF, specifically to compare the similarity of factor profiles across different sites. Figure 3 illustrates the mean and standard deviation of distances between all pairs of factor/source profiles tagged as belonging to the same category in the SID-PD space. This comparison involves  $n \times (n + 1) / 2 - n$  profile pairs for each category, where  $n$  represents the number of profiles assigned to a specific source category (Fig. 3). The results revealed that the chemical profiles for road traffic, secondary sulfate, secondary nitrate, biomass burning, and sea salt exhibit homogeneity across the study sites, indicating their international stability (Fig. 3). In contrast, local sources such as industrial, HOC, and crustal sources showed greater variability in their chemical profiles ( $PD > 0.4$ ), reflecting site- or country-specific differences in these sources (Fig. 3).

Specially, the crustal source may be influenced by desert dust. For example, the DEM\_SUB site is affected by Saharan dust events<sup>33</sup>, which suggests that desert dust might be incorporated into the crustal source without being separately resolved, thereby contributing to the observed variability.

In addition, the analysis of road traffic, secondary sulfate, secondary nitrate, biomass burning, and sea salt profiles confirmed homogeneity across most monitoring sites (see Supplementary Fig. 6). However, variability was observed in the PD-SID results for industrial, HOC, and crustal sources. In detail, for industrial sources, chemical composition varies depending on the specific source at each site. Three sites—MRS-AIX\_UB, MAD-EV\_UB, and GRA\_UB—exhibited substantially different chemical profiles compared to other sites, as indicated by PD values. Regarding HOC, the SID values across all sites remained within the similarity threshold. However, PD analysis revealed differences in the major mass fraction components of this source. The primary component driving these differences in HOC chemical profiles is likely sulfate<sup>36</sup>, which ranged from 0% to 60% across the profiles (see Supplementary Fig. 3). For crustal sources, the chemical profile markers showed clear country-specific characteristics



highlighting that dust profiles are very local and can't be extrapolated easily (in a CTM model for example). While the PD and SID values were generally similar across sites, exceptions were noted for certain locations in Portugal and Spain, such as COIM\_TR, GIJ\_UI, and BAI\_UI. The SID values for all sites were below 1, indicating overall homogeneity in the chemical profiles when considering all components. However, PD values exceeding 0.4 highlight differences in the major mass fraction of crustal dust, likely due to the mixing of road dust and mineral dust.

Additionally, we used the K-W test and Dunn's test to compare temporal relative contributions of the same source type across sites. These analyses found significant differences ( $p < 0.05$ ) between certain site pairs (see Supplementary Tables 3–10). For example, in the case of road traffic sources, CA\_UB exhibited significant differences compared to COIM\_TR, DEM\_SUB, MAG\_UB, ZUR\_UB, MAD-EV\_UB, GRE-fr\_UB, GRE-vif\_UB, LEN\_UB, MRS-LCP\_UB, and MRS-AIX\_UB ( $p < 0.05$ ). These results demonstrate that, while the chemical profiles of road traffic sources are overall similar, their temporal contributions may vary significantly due to local factors such as traffic patterns, meteorological conditions (e.g., thermal inversions in valleys), and emission intensities, leading to localized variability, which could be more accurately captured with higher temporal resolution data, such as daily or hourly measurements.

Similar patterns were observed for other sources. However, when analyzing secondary sulfate, the variability between sites was relatively smaller. Significant differences were only observed between PORT\_TR and other sites, including BAS\_UB, CA\_UB, COIM\_TR, ZUR\_UB, GIJ\_UI, MAD-EV\_UB, CHAM\_UV, GRE-cb\_UB, GRE-fr\_UB, and GRE-vif\_UB. No significant differences were detected among other site pairs, which aligns with the previously discussed observation that sulfate sources tend to be spatially distributed over larger regions<sup>37,38</sup>. This result is due to their formation processes and dispersion characteristics, which result in a more uniform distribution on regional scales.

### Road traffic

Road traffic is a predominant source of PM<sub>10</sub> in urban environments at most monitoring sites. Despite advancements in emission control technologies for both diesel and gasoline vehicle engines, emissions from exhaust (tailpipe) and non-exhaust sources (e.g., tire and brake wear and re-suspended road dust) continue to be significant concerns<sup>28,29,39</sup>. According to the European Environment Agency report, road transport primary emissions contributed to 11% of total PM<sub>10</sub> to the emission inventories in the EU-28 in 2017<sup>40</sup>. In our study, road traffic sources contributions were identified at all sites with contributions to PM<sub>10</sub> ranging from 5% to 41% (Fig. 2). This factor is probably a lower limit since it does not include all the secondary formation of SIA (from NO<sub>2</sub> emissions) nor SOA (from VOC emissions).

At specific sites such as MRS-LCP\_UB, MRS-AIX\_UB, and PORT\_TR, traffic source contributions exceeded 30%, highlighting the substantial impact of road traffic on air quality in these areas. Conversely, sites like MAD-EA\_TR, LEN\_UB, MAG\_UB, and DEM\_SUB had traffic contributions below 10%, suggesting varying levels of traffic-related pollution across different urban settings and locations into a city. The variation in traffic source contributions across different monitoring sites can be attributed to several factors, including the density of vehicular traffic<sup>41</sup>, the effectiveness of local emission control policies<sup>42</sup>, and the urban infrastructure<sup>43</sup>. High traffic density in urban centers typically leads to elevated PM<sub>10</sub> concentrations from both exhaust and non-exhaust emissions. These “non-exhaust” sources contribute as much, and often more, to ambient PM<sub>10</sub> concentrations in cities than tailpipe exhaust<sup>44,45</sup>. Moreover, urban sites near highways or busy intersections tend to show higher pollutant concentrations from the constant vehicular activity. For instance, the higher contributions at MRS-AIX\_UB and MRS-LCP\_UB could be linked to their locations near major traffic routes.

### Biomass burning

Biomass burning is a major source in many regions, contributing substantially to average ambient PM<sub>10</sub> concentrations<sup>46</sup>. Except for BCN\_UB,

biomass burning sources were identified at all other 23 sites, with large variations in their average contributions (10–41%). Specifically, the high contribution at CHAM\_UV, CA\_UB, BAI\_UI, COIM\_UB, COIM\_TR, and MAG\_UB, each exceeding 30%, indicated a substantial impact of biomass burning on local air quality. For example, in the intramountainous valleys of CHAM\_UV, while natural gas is the primary source of household heating<sup>47</sup>, biomass burning (e.g., wood or pellet stoves used as supplementary heating) still contributes substantially to PM<sub>10</sub> concentrations, likely due to cold winter conditions, topographical factors, and traditional heating practices. Conversely, the lower contribution at ZUR\_UB (10%) suggest that the area may have fewer biomass burning activities or have implemented more effective control measures. Therefore, as for road traffic, the substantial contributions in these areas underscore the need for effective management and mitigation strategies to control biomass burning emissions. For the two monitoring sites in Marseille, Longchamp (MRS-LCP\_UB) and Aix-en-Provence (MRS-AIX\_UB), PMF source apportionment identified a mixed source of biomass burning and secondary nitrate, especially during winter and early spring (see Supplementary Fig. 4). This phenomenon is not unique to Marseille but is also observed at other sites where secondary nitrate was identified. This finding aligns with previous study<sup>48</sup> and is typically attributed to lower temperatures and higher relative humidity, which shift the partitioning of semi-volatile ammonium nitrate toward the particle phase<sup>49,50</sup>. Additionally, organic nitrates are an important component of organic aerosols (OA) in Marseille, leading to the mixed source of biogenic aerosols and secondary nitrate<sup>48</sup>.

Furthermore, seasonal variations in biomass burning sources (see Supplementary Fig. 4) show that contributions in winter are generally much higher than in summer for all sites. This is primarily due to increased heating demand and stable atmospheric conditions in winter<sup>51,52</sup>, which intensify the impact of biomass burning.

### Crustal sources

PM<sub>10</sub> contributions from crustal sources were identified at all sites (Fig. 2). Out of the 24 sites, 13 (CHAM\_UV, GRE-cb\_UB, GRE-fr\_UB, GRE-vif\_UB, LEN\_UB, MRS-AIX\_UB, CA\_UB, FLO\_SUB, COIM\_TR, COIM\_UB, BER\_TR, PAY\_UB, and ZUR\_UB) had contributions from crustal sources below 10%. Another 10 sites (MRS-LCP\_UB, DEM\_SUB, PORT\_TR, BCN\_UB, GRA\_UB, MAD-EA\_TR, MAD-EV\_UB, BAS\_UB, and MAG\_UB) showed crustal source contributions ranging from 13% to 17%. However, BAI\_UI and GIJ\_UI had notably higher contributions from crustal sources, at 25% and 33%, respectively. These elevated contributions were primarily due to the influence of the industrial environments around these monitoring sites, especially the ceramic industry near BAI\_UI (Bailen, SE Spain), and various industrial activities around GIJ\_UI (Gijón, Northern Spain). These activities at GIJ\_UI include steel manufacturing (e.g., Arcelor Mittal Ltd.), other metallurgy located in industrial parks or estates (such as Somonte industrial park and Rocas industrial park), the nearby presence of the Aboño Coal-Fired Power Plant, as well as livestock rearing and fisheries<sup>53</sup>. These results indicate that the PM<sub>10</sub> sources at these locations are a mix of crustal and industrial origins, further supporting the earlier observation of chemical profiles where crustal dust tracers co-occur with industrial markers. These findings are also consistent with previous reports on BAI\_UI by de la Campa and de La Rosa<sup>54</sup> and Millán-Martínez et al.<sup>55</sup> and GIJ\_UI by Lara et al.<sup>56</sup> and Megido et al.<sup>57</sup>.

### Industrial sources

Among the 24 monitoring sites, industrial sources were detected at 10 sites (GRE-cb\_UB, GRE-fr\_UB, GRE-vif\_UB, LEN\_UB, MRS-AIX\_UB, COIM\_TR, BAI\_UI, BCN\_UB, GRA\_UB, and MAD-EV\_UB), with contributions ranging from 2% to 14% (Fig. 2). The industrial source contributions at BCN\_UB and COIM\_TR reached 11% and 14% respectively. However, BAI\_UI and GIJ\_UI in known industrial areas, have relatively small industrial source contributions (8% for BAI\_UI) or no detectable industrial sources (0% for GIJ\_UI) (Fig. 2). These results may be partly attributed to the variability in industrial source profiles, which can differ

significantly depending on the types of industrial activities impacting each site. This variability often leads to overlaps between industrial and crustal source profiles, particularly in PMF analysis, where mixed sources may remain unresolved (see Supplementary Fig. 3). For example, industrial processes such as metal smelting, cement production, and chemical manufacturing can produce distinct emissions, making it challenging to define a universal industrial source profile. Consequently, the industrial contributions at sites like BAI\_UI and GIJ\_UI may be underestimated or partially merged with crustal sources, resulting in smaller contributions or the absence of a detectable industrial source. For the other sites (GRE-cb\_UB, GRE-fr\_UB, GRE-vif\_SUB, LEN\_UB, MRS-AIX\_UB, GRA\_UB, and MAD-EV\_UB), the detected industrial source contributions were relatively small (<6%), but they still made contributions to the overall PM<sub>10</sub> pollution pattern. These locations are influenced by small-scale industrial operations and urban activities, which cumulatively contribute to the regional pollution load. Further, the industrial sources' chemical profile generally contains a large fraction of various metals, which can be quite detrimental for public health and generally present large values of oxidative potential<sup>58</sup>.

## Secondary sources

Secondary aerosol sources primarily include secondary nitrates, sulfates, and organic carbon, which are formed through atmospheric reactions involving precursor gases such as nitrogen oxides (NO<sub>x</sub>), sulfur dioxide (SO<sub>2</sub>), and volatile organic compounds (VOCs)<sup>59–62</sup>. These sources exhibit spatial and temporal variability across Europe, influenced by traffic emissions, industrial activities, meteorological conditions, and regional transport.

Specifically, the contribution of secondary nitrates at CHAM\_UV, GRE-cb\_UB, GRE-fr\_UB, GRE-vif\_SUB, LEN\_UB, DEM\_SUB, FLO\_UB, COIM\_UB, MAD-EA\_TR, MAD-EV\_UB, BAS\_UB, BER\_TR, MAG\_UB, PAY\_UB, and ZUR\_UB ranges from 11% to 41% (Fig. 2). Among these, the secondary nitrate contributions at LEN\_UB (Lens, France), BAS\_UB (Basel, Switzerland), PAY\_UB (Payerne, Switzerland), and ZUR\_UB (Zurich, Switzerland) exceed 30%. These values were primarily due to high traffic volumes in these areas, where nitrogen oxides (NO<sub>x</sub>) emitted from vehicles oxidize in the atmosphere to form nitrates<sup>63,64</sup>. Further, the large agricultural activities in northern France and Benelux areas lead to large NH<sub>3</sub> emissions during spring, favoring ammonium nitrate formation<sup>65</sup>. Additionally, certain regions have meteorological conditions, such as low wind speeds, low temperature, and high humidity, that contribute to higher concentrations of semi-volatile substances such as nitrate and ammonium, as observed in Zurich<sup>66</sup> and Basel<sup>67</sup>. This phenomenon aligns with the seasonal variations in secondary nitrate sources identified in this study, which show higher concentrations during the autumn and winter months (see Supplementary Fig. 4).

Secondary sulfate is primarily formed through the oxidation of SO<sub>2</sub> emissions, which are common byproducts of coal and oil combustion<sup>68</sup>. These combustion processes often release pollutants such as Se, As, Pb, V, Ni, and OC. It was previously shown that the inclusion of tracers from secondary biogenic aerosol, like 3-MBTCA, into the PMF could lead to the splitting of a large fraction of OC, particularly in summer, from this sulfate-rich factor into the secondary biogenic factor determined by 3-MBTCA<sup>69</sup>. Representative sites, including CHAM\_UV, GRE-cb\_UB, GRE-fr\_UB, LEN\_UB, MRS-AIX\_UB, CA\_UB, COIM\_TR, PORT\_TR, BCN\_UB, GIJ\_UI, BAS\_UB, BER\_TR, MAG\_UB, and PAY\_UB, show contributions of secondary sulfate and related mixed sources ranging from 5% to 32%, with most sites falling within the moderate range of 15% to 26% (Fig. 2). The mixed sources are primarily linked to HOC (indicated by V and Ni from shipping)<sup>70,71</sup>, coal combustion (indicated by Se, As, and Pb)<sup>72,73</sup>, and regional organic pollutants. Overall, the combined contribution of these two secondary factors (16%–68%) is consistent with previous reports for various urban sites across Europe<sup>74–76</sup>, marking the highest source contribution to PM<sub>10</sub>.

Furthermore, some cities may be affected by the regional transport of PM<sub>10</sub>, where pollutants emitted from surrounding areas contribute to

increased concentrations of secondary sulfates and organic carbon. In contrast, secondary nitrates are primarily formed locally due to the rapid oxidation of NO<sub>2</sub> by OH radicals. Sulfate sources, however, are generally more regional because SO<sub>2</sub> is oxidized approximately ten times more slowly unless the city is near a local source, such as residential coal burning, which can emit primary sulfate directly<sup>77</sup>. This distinction between local and regional contributions highlights the spatial variability in secondary PM sources. For instance<sup>37</sup>, demonstrated that sulfate sources tend to be spatially distributed over larger regions, whereas nitrate sources are often localized.

Overall, the high contribution rates of secondary PM reflect the complexity of abating these pollutants, as they result from a combination of local and regional influences. These findings underscore the need for targeted air quality management strategies that address both local emission reductions (e.g., NO<sub>x</sub> for nitrates) and regional collaboration to manage broader SO<sub>2</sub> and secondary organic aerosol sources effectively.

## Other sources

At the 24 monitoring sites, other specific pollution sources representative of the local emission have also quantitatively identified. One notable source was HOC, primarily detected at sites in Spain, France, Portugal, and Greece. These sites include BCN\_UB, COIM\_UB, GRA\_UB, LEN\_UB, MAD-EV\_UB, MRS-AIX\_UB, MRS-LCP\_UB, DEM\_SUB, MAD-EA\_TR, BAI\_UI, and GIJ\_UI, with contributions ranging from 2% to 15% (Fig. 2).

Another frequently seen source was identified as sea salt, observed at BCN\_UB, MAD-EV\_UB, DEM\_SUB, FLO\_UB, GIJ\_UI, MAD-EA\_TR, and PORT\_TR, contributing from 4% to 21% (Fig. 2). Among these coastal sites, BCN\_UB, PORT\_TR, DEM\_SUB, and GIJ\_UI exhibit contributions exceeding 10%. Sea salt often reflects aged sea salt that contains additional anthropogenic components, such as sulfate and nitrate, from interactions with these acidic pollutants. While sulfate naturally exists in sea salt from seawater, additional sulfate may be introduced through displacement reactions with sulfuric acid or directly on the sea salt particle<sup>78</sup>. As sea salt aerosols age, they undergo chemical reactions with NO<sub>x</sub>, SO<sub>x</sub>, and ammonia in the atmosphere, leading to the formation of secondary inorganic aerosols such as nitrate and sulfate. These reactions not only increase the particle mass but also alter its composition, significantly contributing to PM<sub>10</sub> concentrations. At sites like MRS-AIX\_UB and MRS-LCP\_UB, which are also coastal but where sea salt sources were not explicitly resolved, the absence of measurements for key ions like Na<sup>+</sup> and Cl<sup>−</sup> may explain this limitation. However, the relatively high contributions of secondary sulfates and nitrates at these locations strongly suggest the influence of aged sea salt aerosols, highlighting the need for more comprehensive chemical analyses to better capture their impact. In addition, at the MAD-EV\_UB site, 8% of the PM<sub>10</sub> is attributed to local mines, reflecting the influence of nearby mining activities.

## Marker analysis and source profiles

The identification of major pollution sources was accomplished through the use of specific chemical markers, which allow precise tracing and quantification of contributions from various origins. Road traffic emissions were identified by markers such as EC, OC, Fe, Cr, Mn, Cu, Sb, Sn, Ba, and Zn, while biomass burning was traced using levoglucosan, OC, EC, K, and Rb. Crustal sources were characterized by elements including Ca, Al, K, Mg, Ti, P, Sr, Rb, and Mn, whereas SIA and SOA were associated with markers like NO<sub>3</sub><sup>−</sup>, SO<sub>4</sub><sup>2−</sup>, NH<sub>4</sub><sup>+</sup>, Se, and OC. Industrial emissions were marked by As, Cd, Cr, Cs, Co, Ni, Pb, Rb, Se, V, and Zn, while sea salt sources were dominated by Na or Na<sup>+</sup>, Cl or Cl<sup>−</sup>, Mg or Mg<sup>2+</sup>, often mixed with NO<sub>3</sub><sup>−</sup> and SO<sub>4</sub><sup>2−</sup> due to aging processes. Mixed fuel-oil combustion, including shipping activities, was characterized by V, Ni, SO<sub>4</sub><sup>2−</sup>, and EC. These markers collectively provide a comprehensive understanding of the contributions from various sources across multiple monitoring sites. For example, in the biomass burning source, OC has a high contribution to PM<sub>10</sub>, supporting the significant impact of biomass burning on PM<sub>10</sub> levels. In industrial sources, the higher proportions of metals such as Ni and Zn further support the conclusion that specific industrial sites are influenced by industrial activities.

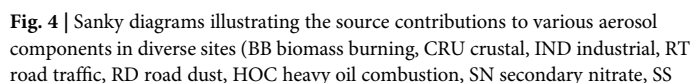
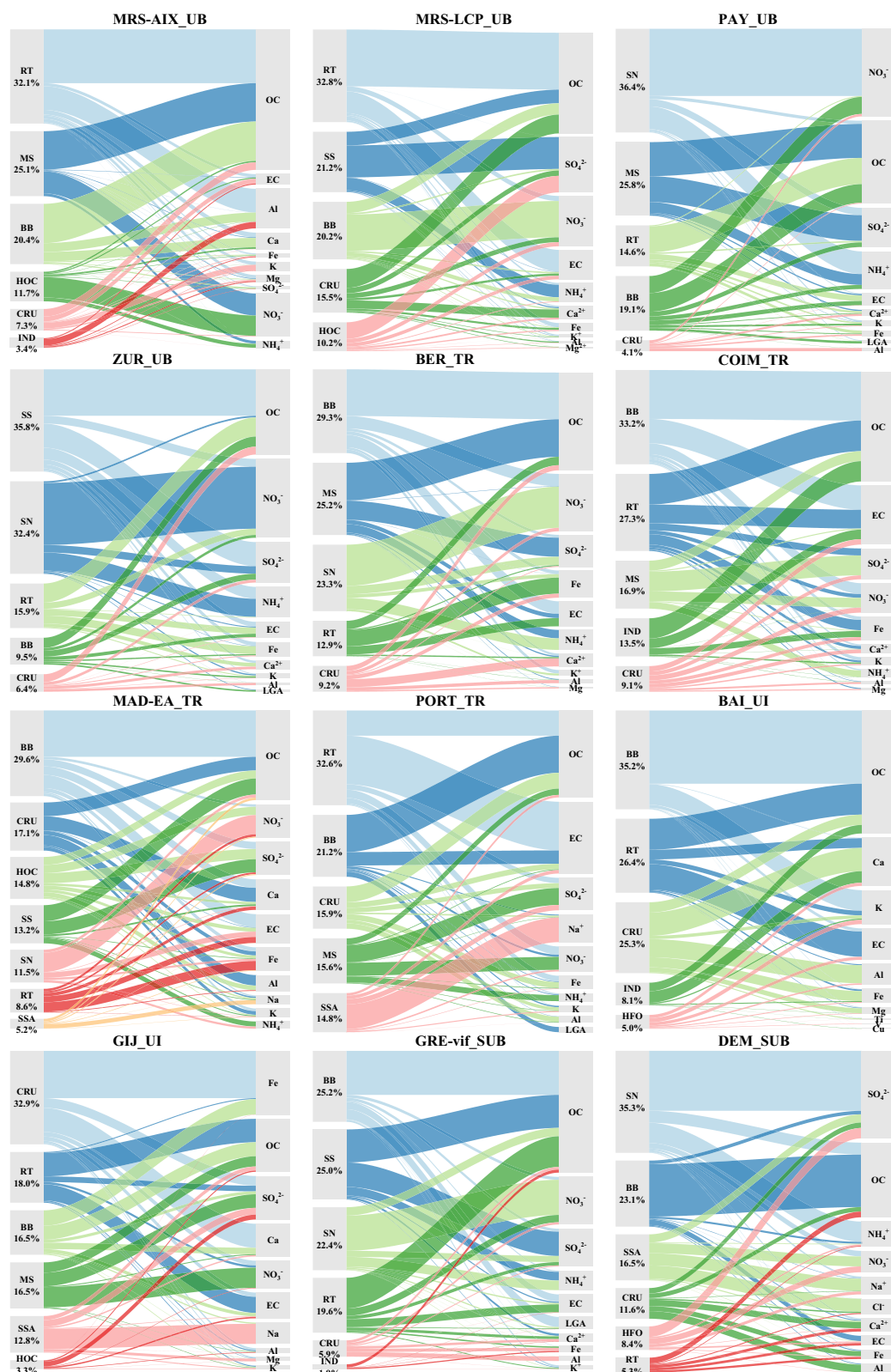


Figure 4 illustrates how chemical components like OC, EC, Cu, Fe, K, and levoglucosan occupy a high proportion in various sources. The factor labeling was made using the same criteria for all the sites to facilitate the assessment of common features and dissimilarities across them.

The results indicated that road traffic emissions were primarily identified by a combination of tracers, each contributing over 40% to the source. Furthermore, Displacement (DISP) analysis revealed that these high concentrations were accompanied by relatively small DISP intervals (see





Supplementary Fig. 7), underscoring the robustness of these findings. This result underscores the significant role of road traffic in air pollution at the monitoring sites. OC was identified as the dominant component in biomass burning, contributing between 27% and 70% of the total biomass burning aerosol, reflecting the source apportionment of PM<sub>10</sub> attributed to biomass combustion. Moreover, the mass of OC represented between  $10 \pm 4\%$  and  $32 \pm 11\%$  of the PM<sub>10</sub> mass during the monitoring period, which is

consistent with prior research<sup>18,75,79</sup>. Regarding the other tracers of biomass burning, levoglucosan and EC were found to account for  $74 \pm 21\%$  and  $43 \pm 10\%$ , respectively, at sites monitoring these markers (levoglucosan at 9 out of 24 sites and EC at 15 out of 24 sites). Mass-wise, levoglucosan and EC contributed  $1 \pm 2\%$  and  $5 \pm 4\%$  to the total PM<sub>10</sub> mass. Additionally, a significant amount of K<sup>+</sup> or K was observed in the biomass burning profile, contributing between 24% and 75% of their respective total mass to this



source (Fig. 4 and Supplementary Fig. 3). These findings further emphasize the substantial impact of biomass burning on PM<sub>10</sub> levels across the monitoring sites.

For crustal sources, with the exception of BAI\_UI and GIJ\_UI, the Sanky diagrams analyses founded that the contributions of Al, Ti, V, Ca<sup>2+</sup> (Ca), Fe, and Mg<sup>2+</sup> (Mg) were the largest within the crustal sources (Fig. 4 and Supplementary Fig. 3). The contributions for these elements ranged from 51%–99% for Al, 35%–85% for Ti, 42%–81% for V, 32%–69% for Ca or Ca<sup>2+</sup>, 34%–74% for Fe, and 32%–75% for Mg or Mg<sup>2+</sup>. These elements are commonly found in crustal material<sup>20</sup> and their high contributions underscore their substantial role in the composition of crustal PM, indicating consistent patterns in PM composition across different geographic locations within Europe. These results align with previous source apportionment findings by Querol et al.<sup>69</sup> and Cesari et al.<sup>80,81</sup>. The considerable presence of crustal sources at various concentrations across all sites emphasizes the importance of implementing urban dust abatement measures in most studied cities. Effective measures might include controlling dust from construction sites, implementing soil conservation practices, maintaining paved roads to reduce soil disturbance<sup>82</sup>, and adopting aggressive street sweeping strategies<sup>83</sup>, as successfully implemented in the US to address urban PM<sub>10</sub> violations<sup>84</sup>. Furthermore, understanding the specific local conditions contributing to higher crustal source emissions can help in tailoring more effective mitigation strategies.

For the two sites with relatively high industrial source contributions (>10%), BCN\_UB and COIM\_TR, as well as the industrial site BAI\_UI, the findings indicate specific industrial influences. In Barcelona (BCN\_UB), industrial sources are primarily characterized by Ni, Cr, Zn, Al, Mn, and Pb, contributing between 27% and 50% to the industrial source (Fig. 4 and Supplementary Fig. 3). This result aligns with previous studies in Barcelona, which have identified these pollutants as being emitted by industrial activities in the southern part of the city, such as smelters and cement kilns<sup>85–87</sup>. Similarly, in Coimbra, Portugal (COIM\_TR), industrial sources are likely linked to the city's smelter and a cement plant located about 8 kilometers northeast of the monitoring site, despite both facilities having emission control measures in place<sup>88</sup>. At the Bailén industrial site (BAI\_UI), high concentrations of Cu were observed, averaging 42 ng/m<sup>3</sup>, with 71% of the Cu attributed to industrial sources (Fig. 4 and Supplementary Fig. 3). This is related to the nearby ceramic industry, as noted in previous research<sup>54,55</sup>. These findings highlight the significant impact of industrial activities on air quality at specific locations and the importance of identifying local industrial sources for effective air quality management.

For secondary sources, the contributions of ammonium, sulfate, nitrate, and organic carbon were observed. Specifically, NO<sub>3</sub><sup>−</sup> contributions ranged from 24% to 83%, SO<sub>4</sub><sup>2−</sup> contributions ranged from 21% to 74%, and NH<sub>4</sub><sup>+</sup> contributions ranged from 26% to 86%. These values were primarily influenced by high traffic volumes in the areas studied, where nitrogen oxides (NO<sub>x</sub>) emitted from vehicles oxidize in the atmosphere to form nitrates. When SO<sub>2</sub> is released into the atmosphere, it undergoes oxidation to form sulfuric acid (H<sub>2</sub>SO<sub>4</sub>), which then reacts with NH<sub>3</sub> to produce ammonium sulfate ((NH<sub>4</sub>)<sub>2</sub>SO<sub>4</sub>), a key component of secondary sulfate aerosols. The same conditions favouring the formation of secondary sulfates (high photochemical oxidation) favour the oxidation of anthropogenic and biogenic volatile organic compounds, which increase secondary organic aerosols simultaneously. The stoichiometric SO<sub>4</sub><sup>2−</sup>/NH<sub>4</sub><sup>+</sup> ratio for (NH<sub>4</sub>)<sub>2</sub>SO<sub>4</sub> is 2.7. In this study, for sites where the secondary sulfate source was individually identified, the SO<sub>4</sub><sup>2−</sup>/NH<sub>4</sub><sup>+</sup> ratio approached the stoichiometric ratio at the following locations: FLO\_UB (3.1), GRA\_UB (2.6), and MRS-LCP\_UB (2.8). However, marine diesels do produce substantial amounts of primary sulfate<sup>89–91</sup> and were identified at multiple European ports by Pandolfi et al.<sup>71</sup>. Strict regulations on SO<sub>2</sub> emissions, such as EU Directives 1999/30/EC, 2008/50/EC<sup>92</sup>, and the amended Directive 89/427/EEC<sup>93</sup>, have led to a significant reduction in SO<sub>2</sub> levels within the European Union. Currently, the primary sources of SO<sub>2</sub> in the EU are emissions from transportation, industry, energy production<sup>94</sup>, district heating<sup>95,96</sup>, and shipping<sup>97,98</sup>, as well as volcanic eruptions<sup>99</sup>.

Additionally, one limitation of PMF is the occurrence of mixed factors, which can result from various factors, such as the sample size and the specific species selected for analysis<sup>100</sup>. For example, secondary sulfate sources are often associated with secondary OC and coal/oil combustion emissions. A prominent mixed source, HOC, is largely influenced by shipping activities. This source is typically marked by V and Ni, with their contributions ranging from 36% to 86% and 21% to 75% in source profiles, respectively (Fig. 4 and Supplementary Fig. 3). These metals are generally present as oxides, though approximately 10% exist as organometallic compounds<sup>101</sup>. This result highlights the impact of maritime transport on air quality in these port regions and presents a challenge to future ship-exhaust source apportionment studies, since HOC emissions must be minimized within Emission Control Areas (ECAs, coastal zones near Europe and North America)<sup>102,103</sup>.

For other pollution sources, sea salt aerosols are predominantly characterized by the ions Na<sup>+</sup> and Cl<sup>−</sup>, which account for 41–94% and 79–86% of the total composition, respectively. These ions are crucial markers of marine influence and provide a clear indication of the contribution of sea salt to atmospheric particulate matter in coastal and marine-adjacent regions. DISP analysis indicated that the high contributions of Na<sup>+</sup> and Cl<sup>−</sup> were associated with narrow DISP intervals (see Supplementary Fig. 6), further validating their reliability as tracers of sea salt aerosols.

## Materials and methods

### Study area

All datasets in this study provide PM<sub>10</sub> chemical speciation. Of the 24 selected sites, 18 are located in background locations, including 16 urban backgrounds (UB) and 2 suburban backgrounds (SUB). The remaining sites were specifically chosen for urban traffic (TR) (4/24) and urban industry (UI) (2/24) context. These monitoring sites are spread across 6 European countries and provide data for 3,602 samples: France (7 sites), Greece (1), Italy (2), Portugal (3), Spain (6), and Switzerland (5) (see Supplementary Fig. 8 and list below). Each site has at least one year of data to ensure its representativeness (see Supplementary Table 11). For a detailed description of the sampling sites and the analytical techniques employed, please refer to Liu et al.<sup>9</sup>.

- Sixteen urban background (UB) sites: Basel (BAS\_UB), Barcelona (BCN\_UB), Capannori Lucca (CA\_UB), Coimbra (COIM\_UB), Florence Firenze\_Bassi (FLO\_UB), Granada (GRA\_UB), Grenoble CB (GRE-cb\_UB), Grenoble FR (GRE-fr\_UB), Lens (LEN\_UB), Madrid E. Vallecas (MAD-EV\_UB), Magadino (MAG\_UB), Marseille Longchamp (MRS-LCP\_UB), Aix-en-Provence (MRS-AIX\_UB), Payerne (PAY\_UB), Zurich (ZUR\_UB), Chamonix (CHAM\_UB), with UV referring to UB sites in intra-mountainous valleys).
- Four traffic (TR) sites: Bern (BER\_TR), Coimbra (COIM\_TR), Madrid Esc. Aguirre (MAD-EA\_TR), Porto (PORT\_TR).
- Two urban industrial (UI) sites: Bailen (BAI\_UI) and Gijon/Aviles (GIJ\_UI).
- Two suburban sites: Athens Demokritos (DEM\_SUB) and Grenoble VIF (GRE-vif\_SUB).

### Chemical analyses

The instrumentation used for measuring the chemistry of PM<sub>10</sub> at the different stations is described in Supplementary Table 1. Briefly, in this study, the elements (Na, Mg, Al, K, Ca, Ti, V, Cr, Mn, Fe, Ni, Cu, Zn, As, Se, Rb, Cd, Sn, Sb, Ba, and Pb) were measured by (i) Inductively Coupled Plasma-Mass Spectrometry (ICP-MS), (ii) Particle Induced X-Ray Emission (PIXE) and (iii) X-Ray Fluorescence (XRF). More details can be found in Liu et al.<sup>9</sup>. The Water-soluble ions (Ca<sup>2+</sup>, K<sup>+</sup>, Mg<sup>2+</sup>, SO<sub>4</sub><sup>2−</sup>, NO<sub>3</sub><sup>−</sup>, and NH<sub>4</sub><sup>+</sup>) were quantified with ion chromatographs (ICs). The organic (OC) and elemental (EC) carbon were analyzed by a Thermal-Optical-Transmission method (Sunset Lab., OR, US) using the EUSAAR\_2 protocol<sup>104</sup>. To enhance the quantification of biomass burning sources, levoglucosan was monitored at several sites by determining its concentration by means of Gas Chromatography-Mass Spectrometry (GC-MS) or high-performance liquid chromatography

analysis tandem photodiode array detection (HPLC-PAD), for the sites of COIM\_UB, GIJ\_UI, GRE-fr\_UB, GRE-vif\_SUB, MAD-EV\_UB, PAY\_UB, ZUR\_UB, MAD-EA\_TR, and PORT\_TR.

### Quality assurance and quality control procedures

A comprehensive set of quality assurance and quality control (QA/QC) protocols was implemented across all analytical techniques. These procedures included the routine submission and analysis of field blanks, the exclusion of compromised or damaged filters, and the pre-analysis optimization of instruments such as ICP-MS, PIXE, and XRF. Regular assessments of filter blanks were conducted to ensure accurate blank corrections from the measured concentrations. Additionally, a maximum threshold was established for the standard deviation of five internal-standard-corrected signal intensities for each sample during every analytical run. On average, the standard deviation for final results fell within the range of 5–10%; however, for certain elements, particularly those with lower concentrations or those analyzed by specific instruments, this value could increase, reaching up to approximately 20%. More details have been described in our previous study<sup>9</sup>.

### Data selection and preprocessing

PMF has been widely utilized in analyzing PM sources during the last decades<sup>105–107</sup>. It is a multivariate factor analysis receptor model, dividing the speciated sample data matrix into two matrices: factor contributions and factor profiles. In the present study, the EPA PMF v.5.0 has been used<sup>108</sup>. Detailed descriptions of PMF and result diagnostics can be found in Paatero and Tapper (1994); Hopke, Paatero et al.<sup>106,109–112</sup>.

Species were selected based on two criteria: (1) a minimum detection frequency of 80% and (2) signal-to-noise ratio (S/N), calculated as the mean difference between concentration and uncertainty divided by the uncertainty. Across all sites, all collected species met the 80% detection threshold, and the species list was narrowed to 17–28 per site after S/N screening, based on detection frequency and uncertainty (see Supplementary Fig. 9).

A few samples were excluded before model input due to anomalous events (e.g., fireworks during holidays such as Christmas or New Year's Day), as these do not represent typical emission patterns<sup>113,114</sup>. In addition, all datasets were processed by the same analyst, including outlier screening and the PMF analysis (e.g., standardized criteria used during the source apportionment process).

### Uncertainty estimation

The uncertainties were treated as follows:

- Data below the limit of quantification (LOQ) were replaced with half of the LOQ and the uncertainties were set to 5/6 of the LOQ<sup>115</sup>. The LOQ values for each factor at different sites are provided in Supplementary Table 12.
- The uncertainties (*u*) of the other data were set according to Eq. (1)

$$u = \left[ (\text{error fraction} \times \text{concentration})^2 + (0.05 \times \text{LOQ})^2 \right]^{0.5} \quad (1)$$

where error fraction is the fraction of uncertainty, LOQ is the limit of quantification<sup>108</sup>. Error fraction was estimated from sampling error and analytical error. In PMF analysis we assumed error fractions of 10% for each metric.

In principle, PMF has the ability to model peaks concentrations reasonably well. In the present study.

### PMF execution and model validation

To determine the optimal number of factors, we started by varying the number of factors in PMF from 2 to 9. In this study, S/N ratio are as follows: “strong” if  $S/N > 1$ , “weak” if  $0.5 \leq S/N \leq 1$ , and “bad” if  $S/N < 0.5$ . However, if a species was critical for identifying a specific source, S/N thresholds were reconsidered (e.g., reassigning weak or bad to strong). Diagnostic parameters such as Pearson correlation coefficients ( $R^2$ , representing the

coefficient of determination between observed and modeled concentrations for each species) were categorized as “strong” if  $R^2 > 0.6$ , “weak” if  $R^2 < 0.6$ . Conversely, species with significant relative contributions but less importance to source identification were adjusted to weak or bad. Within this range, further evaluation of source profiles and matrices determined the final solution. Additional diagnostics such as  $Q_{\text{true}}$ ,  $Q_{\text{robust}}$ ,  $Q_{\text{true}}/Q_{\text{expect}}$ , interpretability of factor profiles, and the possibility of the temporal variations of source contributions were calculated to jointly identify the optimal solution as exemplified in Glojek et al.<sup>116</sup> (see Supplementary Figs. 3, 4, 10 and 11). The final selection for each site combined these criteria to ensure robust solutions.

Model robustness was further tested using DISP (displacement analysis) and BS (bootstrap) methods, which were used to confirm the robustness and uniqueness of the PMF solutions<sup>112,117</sup> (see Supplementary Fig. 7 and Supplementary Table 13). No factor swaps were reported within the allowed dQmax range. While correlations between BS runs and base factors varied, a substantial portion reached or exceeded 80%. Potential sources were interpreted based on seasonal and geochemical considerations<sup>117</sup>. This approach ensured that PMF analyses were robust, with solutions that accurately captured source contributions across monitoring sites.

### Sensitivity analysis of below-LOQ treatment

To assess the potential impact of handling data below the LOQ on the stability and interpretability of PMF results—especially for trace species such as Ni and levoglucosan that are important for source identification—we conducted a sensitivity analysis using data from representative Swiss sites (BAS\_UB, BER\_TR, MAG\_UB, and ZUE\_UB). Two aspects were tested: (1) concentration substitution, by comparing the standard 1/2 LOQ replacement with full LOQ values for below-LOQ data; and (2) uncertainty estimation, by evaluating three scenarios in which uncertainties for these data were set to 1/2 LOQ, 5/6 LOQ, or full LOQ.

Across both tests, PMF yielded consistent source contributions, suggesting that the treatment of below-LOQ values had a minimal effect on the overall resolution and reliability of the model outputs. These findings support the robustness of the PMF results and are further documented in Supplementary Fig. 12.

### Similarity assessment

To assess the similarity between the chemical source profiles across European sites, comparisons were made based on the specific chemical relative mass composition at each location, using the Pearson distance (PD) and standardized identity distance (SID) metrics. These distances help evaluate the homogeneity of the source chemical profiles across different urban settings. Calculations for PD and SID were described by Belis et al.<sup>35</sup> with the equations presented below:

$$PD = 1 - R^2 \quad (2)$$

where  $R^2$  is the Pearson coefficient of the relative mass to PM of all components between 2 sites.

$$SID = \frac{\sqrt{2}}{m} \sum_{j=1}^m \frac{|x_j - y_j|}{x_j + y_j} \quad (3)$$

where  $m$  is the number of chemical compositions in a source,  $x$  and  $y$  are the relative mass to PM of 2 different factors or sources.

The PD metric primarily indicates the sensitivity of a chemical profile to variations in the main mass fractions of particulate matter, while the SID reflects sensitivity to the entire range of components, including trace species. Profiles that are consistent across various site types are generally expected to have PD values below 0.4 and SID values below 1.0<sup>118</sup>. In contrast, profiles with values exceeding these thresholds are considered heterogeneous.

## Data availability

This study used existing datasets on PM<sub>10</sub> chemical speciation collected from 24 monitoring sites across six European countries. These datasets were previously described in detail in Liu et al.<sup>9</sup>. No new datasets were generated in this study. The data were used for secondary analysis, including pre-processing and PMF modeling. Further details on data processing, quality control procedures, and species selection are provided in the manuscript and Supplementary Information. Data access is subject to the original data providers' policies.

Received: 4 February 2025; Accepted: 20 May 2025;

Published online: 05 July 2025

## References

- Cohen, A. J. et al. Estimates and 25-year trends of the global burden of disease attributable to ambient air pollution: an analysis of data from the global burden of diseases study 2015. *Lancet* **389**, 1907–1918 (2017).
- Lelieveld, J. et al. Loss of life expectancy from air pollution compared to other risk factors: a worldwide perspective. *Cardiovasc. Res.* **116**, 1910–1917 (2020).
- WHO. *WHO Global Air Quality Guidelines 2021 World Health Organization* (WHO, 2021).
- Nagar, J. K., Akolkar, A. B. & Kumar, R. A review on airborne particulate matter and its sources, chemical composition and impact on human respiratory system. *Int. J. Environ. Sci.* **5**, 447–463 (2014).
- Directive. Directive (EU) 2024/2881 of the European Parliament and of the Council of 23 October 2024 on ambient air quality and cleaner air for Europe (recast). *Official J. Eur. Union* (2024).
- Aas, W. et al. Trends in air pollution in Europe, 2000–2019 (2024).
- Hforouzanfar, M. et al. Global, regional, and national comparative risk assessment of 79 behavioural, environmental and occupational, and metabolic risks or clusters of risks, 1990–2015: a systematic analysis for the global burden of disease study 2015. *Lancet* **388**, 1659–1724 (2016).
- Fowler, D. et al. A chronology of global air quality. *Philos. Trans. R. Soc. A* **378**, 20190314 (2020).
- Liu, X. et al. PM<sub>10</sub>-bound trace elements in pan-European urban atmosphere. *Environ. Res.* **260**, 119630 (2024).
- Daellenbach, K. R. et al. Sources of particulate-matter air pollution and its oxidative potential in Europe. *Nature* **587**, 414–419 (2020).
- Viana, M. et al. Source apportionment of particulate matter in Europe: a review of methods and results. *J. Aerosol Sci.* **39**, 827–849 (2008).
- Hopke, P. K., Dai, Q., Li, L. & Feng, Y. Global review of recent source apportionments for airborne particulate matter. *Sci. Total Environ.* **740**, 140091 (2020).
- Canha, N. et al. Pollution sources affecting the oxidative potential of fine aerosols in a Portuguese urban-industrial area—an exploratory study. *Air Quality Atmos. Health* **17**, 2005–2015 (2024).
- Sánchez, E. P. et al. Improving air pollution source apportionment in size-segregated pm using Pb isotope-based Bayesian mixing models in Tarragona (Spain). *Atmos. Res.* **316**, 107939 (2025).
- Srivastava, D. et al. Comparative receptor modelling for the sources of fine particulate matter (PM<sub>2.5</sub>) at urban sites in the UK. *Atmos. Environ.* **343**, 120963 (2025).
- van Pinxteren, D. et al. Residential wood combustion in Germany: a twin-site study of local village contributions to particulate pollutants and their potential health effects. *ACS Environ. Au* **4**, 12–30 (2023).
- Harni, S. D. et al. Source apportionment of particle number size distribution at the street canyon and urban background sites. *Atmos. Chem. Phys.* **24**, 12143–12160 (2024).
- Weber, S. et al. Comparison of PM<sub>10</sub> sources profiles at 15 French sites using a harmonized constrained positive matrix factorization approach. *Atmosphere* **10**, 310 (2019).
- Grange, S. K. et al. Switzerland's PM<sub>10</sub> and PM<sub>2.5</sub> environmental increments show the importance of non-exhaust emissions. *Atmos. Environ. X* **12**, 100145 (2021).
- Querol, X. et al. PM<sub>10</sub> and PM<sub>2.5</sub> source apportionment in the Barcelona metropolitan area, Catalonia, Spain. *Atmos. Environ.* **35**, 6407–6419 (2001).
- Kim, E. & Hopke, P. K. Source apportionment of fine particles in Washington, DC, utilizing temperature-resolved carbon fractions. *J. Air Waste Manag. Assoc.* **54**, 773–785 (2004).
- Amato, F. et al. Airuse-life + : a harmonized pm speciation and source apportionment in five southern European cities. *Atmos. Chem. Phys.* **16**, 3289–3309 (2016).
- Liang, C., Duan, F., He, K. & Ma, Y. Review on recent progress in observations, source identifications and countermeasures of PM<sub>2.5</sub>. *Environ. Int.* **86**, 150–170 (2016).
- Dunn, O. J. Multiple comparisons using rank sums. *Technometrics* **6**, 241–252 (1964).
- Kruskal, W. H. & Wallis, W. A. Use of ranks in one-criterion variance analysis. *J. Am. Stat. Assoc.* **47**, 583–621 (1952).
- Zhong, C. et al. Ecological geochemical assessment and source identification of trace elements in atmospheric deposition of an emerging industrial area: Beibu Gulf Economic Zone. *Sci. Total Environ.* **573**, 1519–1526 (2016).
- Samek, L. et al. Seasonal variations of chemical composition of pm<sub>2.5</sub> fraction in the urban area of krakow, poland: pmf source attribution. *Air Qual. Atmos. Health* **13**, 89–96 (2020).
- Demir, T., Karakaş, D. & Yenisoy-Karakaş, S. Source identification of exhaust and non-exhaust traffic emissions through the elemental carbon fractions and positive matrix factorization method. *Environ. Res.* **204**, 112399 (2022).
- Charron, A. et al. Identification and quantification of particulate tracers of exhaust and non-exhaust vehicle emissions. *Atmos. Chem. Phys.* **19**, 5187–5207 (2019).
- Pey, J., Querol, X. & Alastuey, A. Discriminating the regional and urban contributions in the north-western mediterranean: pm levels and composition. *Atmos. Environ.* **44**, 1587–1596 (2010).
- Grivas, G., Cheristanidis, S., Chaloulakou, A., Koutrakis, P. & Mihalopoulos, N. Elemental composition and source apportionment of fine and coarse particles at traffic and urban background locations in Athens, Greece. *Aerosol Air Qual. Res.* **18**, 1642–1659 (2018).
- Eleftheriadis, K., Balis, D., Ziomans, I. C., Colbeck, I. & Manalis, N. Atmospheric aerosol and gaseous species in Athens, Greece. *Atmos. Environ.* **32**, 2183–2191 (1998).
- Vasilatou, V. et al. Characterization of PM<sub>2.5</sub> chemical composition at the Demokritos suburban station, in Athens, Greece. The influence of Saharan dust. *Environ. Sci. Pollut. Res.* **24**, 11836–11846 (2017).
- Hopke, P. K., Feng, Y. & Dai, Q. Source apportionment of particle number concentrations: a global review. *Sci. Total Environ.* **819**, 153104 (2022).
- Belis, C. A. et al. A new methodology to assess the performance and uncertainty of source apportionment models in intercomparison exercises. *Atmos. Environ.* **119**, 35–44 (2015).
- Fossum, K. N. et al. Two distinct ship emission profiles for organic-sulfate source apportionment of pm in sulfur emission control areas. *Atmos. Chem. Phys.* **24**, 10815–10831 (2024).
- Zhao, W., Hopke, P. K. & Zhou, L. Spatial distribution of source locations for particulate nitrate and sulfate in the upper-midwestern United States. *Atmos. Environ.* **41**, 1831–1847 (2007).
- Ying, Q., Wu, L. & Zhang, H. Local and inter-regional contributions to PM<sub>2.5</sub> nitrate and sulfate in China. *Atmos. Environ.* **94**, 582–592 (2014).
- Alves, C. A. et al. Size-segregated particulate matter and gaseous emissions from motor vehicles in a road tunnel. *Atmos. Res.* **153**, 134–144 (2015).



40. EEA. *Air Quality in Europe—2019 Report* (European Environment Agency, 2019).
41. Liu, X. et al. Levels and drivers of urban black carbon and health risk assessment during pre-and Covid19 lockdown in Augsburg, Germany. *Environ. Pollut.* **316**, 120529 (2022).
42. Cao, X. et al. Investigation of COVID-19-related lockdowns on the air pollution changes in Augsburg in 2020, Germany. *Atmos. Pollut. Res.* **13**, 101536 (2022).
43. Jafarigol, F. et al. The relative contributions of traffic and non-traffic sources in ultrafine particle formations in Tehran megacity. *Sci. Rep.* **14**, 10399 (2024).
44. Amato, F. et al. Urban air quality: the challenge of traffic non-exhaust emissions. *J. Hazard. Mater.* **275**, 31–36 (2014).
45. Piscitello, A., Bianco, C., Casasso, A. & Sethi, R. Non-exhaust traffic emissions: sources, characterization, and mitigation measures. *Sci. Total Environ.* **766**, 144440 (2021).
46. Jiang, K. et al. Pollutant emissions from biomass burning: a review on emission characteristics, environmental impacts, and research perspectives. *Particuology* **85**, 296–309 (2023).
47. Brulfert, G. et al. Assessment of 2010 air quality in two alpine valleys from modelling: weather type and emission scenarios. *Atmos. Environ.* **40**, 7893–7907 (2006).
48. Chazeau, B. et al. Measurement report: fourteen months of real-time characterisation of the submicronic aerosol and its atmospheric dynamics at the marseille-longchamp supersite. *Atmos. Chem. Phys.* **21**, 7293–7319 (2021).
49. Stelson, A. W. & Seinfeld, J. H. Relative humidity and temperature dependence of the ammonium nitrate dissociation constant. *Atmos. Environ.* **16**, 983–992 (1982).
50. Huffman, J. A. et al. Chemically-resolved aerosol volatility measurements from two megacity field studies. *Atmos. Chem. Phys.* **9**, 7161–7182 (2009).
51. Liu, X. et al. Combined land-use and street view image model for estimating black carbon concentrations in urban areas. *Atmos. Environ.* **265**, 118719 (2021).
52. Liu, X. et al. Spatiotemporal characteristics and driving factors of black carbon in Augsburg, Germany: combination of mobile monitoring and street view images. *Environ. Sci. Technol.* **55**, 160–168 (2021).
53. Nieto, P. G. & Antón, J. Á Nonlinear air quality modeling using multivariate adaptive regression splines in gijón urban area (northern Spain) at local scale. *Appl. Math. Comput.* **235**, 50–65 (2014).
54. de la Campa, A. S. & de La Rosa, J. D. Implications for air quality and the impact of financial and economic crisis in south Spain: geochemical evolution of atmospheric aerosol in the ceramic region of bailén. *Atmos. Environ.* **98**, 519–529 (2014).
55. Millán-Martínez, M., Sánchez-Rodas, D., de la Campa, A. M. S. & de la Rosa, J. Contribution of anthropogenic and natural sources in PM10 during north African dust events in southern Europe. *Environ. Pollut.* **290**, 118065 (2021).
56. Lara, R. et al. Health risk assessment of potentially toxic elements in the dry deposition fraction of settleable particulate matter in urban and suburban locations in the city of Gijón, Spain. *J. Environ. Chem. Eng.* **9**, 106794 (2021).
57. Megido, L. et al. Enrichment factors to assess the anthropogenic influence on PM10 in Gijón (Spain). *Environ. Sci. Pollut. Res.* **24**, 711–724 (2017).
58. Weber, S. et al. Source apportionment of atmospheric pm 10 oxidative potential: synthesis of 15 year-round urban datasets in France. *Atmos. Chem. Phys.* **21**, 11353–11378 (2021).
59. Wang, Z. et al. Enhanced heterogeneous uptake of sulfur dioxide on mineral particles through modification of iron speciation during simulated cloud processing. *Atmos. Chem. Phys.* **19**, 12569–12585 (2019).
60. Tomasi, C. & Lupi, A. in *Atmospheric Aerosols: Life Cycles and Effects on Air Quality and Climate* (eds Tomasi, C., Fuzzi, S. & Kokhanovsky, A.) 1–86 (John Wiley & Sons, 2017).
61. Wang, T. et al. The influence of temperature on the heterogeneous uptake of SO<sub>2</sub> on hematite particles. *Sci. Total Environ.* **644**, 1493–1502 (2018).
62. Wang, T. et al. Key factors determining the formation of sulfate aerosols through multiphase chemistry—a kinetic modeling study based on Beijing conditions. *J. Geophys. Res.: Atmos.* **128**, e2022J–e38382J (2023).
63. Plauchu, R. et al. NO<sub>x</sub> emissions in France in 2019–2021 as estimated by the high-spatial-resolution assimilation of tropomi no 2 observations. *Atmos. Chem. Phys.* **24**, 8139–8163 (2024).
64. Ren, C. et al. Nonlinear response of nitrate to NO<sub>x</sub> reduction in China during the COVID-19 pandemic. *Atmos. Environ.* **264**, 118715 (2021).
65. Favez, O. et al. Overview of the French operational network for in situ observation of pm chemical composition and sources in urban environments (Cara program). *Atmosphere* **12**, 207 (2021).
66. Fisseha, R. et al. Seasonal and diurnal characteristics of water soluble inorganic compounds in the gas and aerosol phase in the Zurich area. *Atmos. Chem. Phys.* **6**, 1895–1904 (2006).
67. Rössli, M. et al. Temporal and spatial variation of the chemical composition of PM10 at urban and rural sites in the Basel area, Switzerland. *Atmos. Environ.* **35**, 3701–3713 (2001).
68. Jafarnejad, S. Control and treatment of sulfur compounds specially sulfur oxides (SO<sub>x</sub>) emissions from the petroleum industry: a review. *Chem. Int.* **2**, 242–253 (2016).
69. Borlaza, L. J. S. et al. Disparities in particulate matter (pm 10) origins and oxidative potential at a city scale (Grenoble, France)—part 1: source apportionment at three neighbouring sites. *Atmos. Chem. Phys.* **21**, 5415–5437 (2021).
70. Becagli, S. et al. Evidence for heavy fuel oil combustion aerosols from chemical analyses at the island of Lampedusa: a possible large role of ships emissions in the Mediterranean. *Atmos. Chem. Phys.* **12**, 3479–3492 (2012).
71. Pandolfi, M. et al. Long-range and local air pollution: what can we learn from chemical speciation of particulate matter at paired sites?. *Atmos. Chem. Phys.* **20**, 409–429 (2020).
72. Querol, X., Fernández-Turiel, J. & López-Soler, A. Trace elements in coal and their behaviour during combustion in a large power station. *Fuel* **74**, 331–343 (1995).
73. Pokorná, P. et al. Comparison of PM2.5 chemical composition and sources at a rural background site in central Europe between 1993/1994/1995 and 2009/2010: effect of legislative regulations and economic transformation on the air quality. *Environ. Pollut.* **241**, 841–851 (2018).
74. Beuck, H., Quass, U., Klemm, O. & Kuhlbusch, T. Assessment of sea salt and mineral dust contributions to PM10 in NW Germany using tracer models and positive matrix factorization. *Atmos. Environ.* **45**, 5813–5821 (2011).
75. Belis, C. A., Karagulian, F., Larsen, B. R. & Hopke, P. K. Critical review and meta-analysis of ambient particulate matter source apportionment using receptor models in Europe. *Atmos. Environ.* **69**, 94–108 (2013).
76. Waked, A. et al. Source apportionment of PM10 in a north-western Europe regional urban background site (Lens, France) using positive matrix factorization and including primary biogenic emissions. *Atmos. Chem. Phys.* **14**, 3325–3346 (2014).
77. Dai, Q. et al. Residential coal combustion as a source of primary sulfate in Xi'an, China. *Atmos. Environ.* **196**, 66–76 (2019).
78. Su, B. et al. A review of atmospheric aging of sea spray aerosols: potential factors affecting chloride depletion. *Atmos. Environ.* **290**, 119365 (2022).



79. Schauer, J. J., Kleeman, M. J., Cass, G. R. & Simoneit, B. R. Measurement of emissions from air pollution sources. 3. C1 – c29 organic compounds from fireplace combustion of wood. *Environ. Sci. Technol.* **35**, 1716–1728 (2001).
80. Querol, X. et al. Speciation and origin of PM10 and PM2.5 in selected European cities. *Atmos. Environ.* **38**, 6547–6555 (2004).
81. Cesari, D. et al. An inter-comparison of PM10 source apportionment using PCA and PMF receptor models in three European sites. *Environ. Sci. Pollut. Res.* **23**, 15133–15148 (2016).
82. Sager, M. Urban soils and road dust—civilization effects and metal pollution—a review. *Environments* **7**, 98 (2020).
83. Amato, F., Querol, X., Johansson, C., Nagl, C. & Alastuey, A. A review on the effectiveness of street sweeping, washing and dust suppressants as urban pm control methods. *Sci. Total Environ.* **408**, 3070–3084 (2010).
84. Calvillo, S. J., Williams, E. S. & Brooks, B. W. Street dust: implications for stormwater and air quality, and environmental management through street sweeping. *Rev. Environ. Contamination Toxicol.* **ume 233**, 71–128 (2014).
85. Amato, F. et al. Quantifying road dust resuspension in urban environment by multilinear engine: a comparison with pmf2. *Atmos. Environ.* **43**, 2770–2780 (2009).
86. Minguillón, M. C. et al. Source apportionment of indoor, outdoor and personal PM2.5 exposure of pregnant women in barcelona, spain. *Atmos. Environ.* **59**, 426–436 (2012).
87. Minguillón, M. C. et al. Spatial variability of trace elements and sources for improved exposure assessment in barcelona. *Atmos. Environ.* **89**, 268–281 (2014).
88. Lourenço, A. M. & Gomes, C. R. Integration of magnetic measurements, chemical and statistical analysis in characterizing agricultural soils (central portugal). *Environ. Earth Sci.* **75**, 1–17 (2016).
89. Agrawal, H., Welch, W. A., Miller, J. W. & Cocker, D. R. Emission measurements from a crude oil tanker at sea. *Environ. Sci. Technol.* **42**, 7098–7103 (2008).
90. Agrawal, H., Malloy, Q. G., Welch, W. A., Miller, J. W. & Cocker III, D. R. In-use gaseous and particulate matter emissions from a modern ocean going container vessel. *Atmos. Environ.* **42**, 5504–5510 (2008).
91. Agrawal, H., Welch, W. A., Henningsen, S., Miller, J. W. & Cocker III, D. R. Emissions from main propulsion engine on container ship at sea. *J. Geophys. Res.: Atmos.* **115** (2010).
92. Eu. Directive 2008/50/EC of the European Parliament and of the Council of 21 May 2008 on ambient air quality and cleaner air for Europe. *Official J. Eur. Union* (2008).
93. Eu. Council Directive 1999/30/EC of 22 April 1999 relating to limit values for sulphur dioxide, nitrogen dioxide and oxides of nitrogen, particulate matter and lead in ambient air (1999).
94. Shen, G. et al. Contributions of biomass burning to global and regional SO<sub>2</sub> emissions. *Atmos. Res.* **260**, 105709 (2021).
95. Radović, B., Ilić, P., Popović, Z., Vuković, J. & Smiljanić, S. Air quality in the town of Bijeljina- trends and levels of SO<sub>2</sub> and NO<sub>2</sub> concentrations. *Qual. Life (Banja Luka)-Apeiron* **22**, 46–57 (2022).
96. Syrek-Gerstenkorn, Z., Syrek-Gerstenkorn, B. & Paul, S. A comparative study of SO<sub>x</sub>, NO<sub>x</sub>, PM2.5 and PM10 in the UK and Poland from 1970 to 2020. *Appl. Sci.* **14**, 3292 (2024).
97. Serbula, S. M. et al. Arsenic and SO<sub>2</sub> hotspot in south-eastern Europe: an overview of the air quality after the implementation of the flash smelting technology for copper production. *Sci. Total Environ.* **777**, 145981 (2021).
98. Lee, J., Pasternak, D., Wilde, S. & Lacy, S. SO<sub>2</sub> and NO<sub>x</sub> emissions from European shipping: a measurement study. In *EGU General Assembly Conference Abstracts*, 10092 (2024).
99. Inness, A. et al. Evaluating the assimilation of s5p/tropomi near real-time SO<sub>2</sub> columns and layer height data into the CAMS integrated forecasting system (cy47r1), based on a case study of the 2019 Raikoke eruption. *Geosci. Model Dev.* **15**, 971–994 (2022).
100. Saraga, D. et al. Multi-city comparative PM2.5 source apportionment for fifteen sites in Europe: the Icarus project. *Sci. Total Environ.* **751**, 141855 (2021).
101. Corbin, J. C. et al. Trace metals in soot and PM2.5 from heavy-fuel-oil combustion in a marine engine. *Environ. Sci. Technol.* **52**, 6714–6722 (2018).
102. Czech, H., Schnelle-Kreis, J., Streibel, T. & Zimmermann, R. New directions: beyond sulphur, vanadium and nickel—about source apportionment of ship emissions in emission control areas. *Atmos. Environ.* **163**, 190–191 (2017).
103. Anastasopoulos, A. T. et al. Evaluating the effectiveness of low-sulphur marine fuel regulations at improving urban ambient PM2.5 air quality: source apportionment of PM2.5 at Canadian Atlantic and Pacific coast cities with implementation of the North American Emissions Control Area. *Sci. Total Environ.* **904**, 166965 (2023).
104. Cavalli, F., Viana, M., Yttri, K. E., Genberg, J. & Putaud, J. Toward a standardised thermal-optical protocol for measuring atmospheric organic and elemental carbon: the eusaar protocol. *Atmos. Meas. Tech.* **3**, 79–89 (2010).
105. Paatero, P. & Tapper, U. Analysis of different modes of factor analysis as least squares fit problems. *Chemometrics Intell. Lab. Syst.* **18**, 183–194 (1993).
106. Paatero, P. & Tapper, U. Positive matrix factorization: a non-negative factor model with optimal utilization of error estimates of data values. *Environmetrics* **5**, 111–126 (1994).
107. Paatero, P. & Hopke, P. K. Rotational tools for factor analytic models. *J. Chemometrics* **23**, 91–100 (2009).
108. Norris, G., Duvall, S., Brown, S. & Bai, S. Epa positive matrix factorization (PMF) 5.0. In: fundamentals and user guide. Epa/600/r-14/108 (ntis pb2015-105147) (2014). <http://www.epa.gov/heads/products/pmf/pmf.html>.
109. Hopke, P. K. A guide to positive matrix factorization. In: *Proc. Workshop on UNMIX and PMF as Applied to PM2*, 6002000.
110. Paatero, P., Hopke, P. K. & Song, X. & Ramadan, Z. Understanding and controlling rotations in factor analytic models. *Chemometrics Intell. Lab. Syst.* **60**, 253–264 (2002).
111. Paatero, P., Hopke, P. K., Hoppenstock, J. & Eberly, S. I. Advanced factor analysis of spatial distributions of pm2. 5 in the eastern united states. *Environ. Sci. Technol.* **37**, 2460–2476 (2003).
112. Paatero, P., Eberly, S., Brown, S. G. & Norris, G. A. Methods for estimating uncertainty in factor analytic solutions. *Atmos. Meas. Tech.* **7**, 781–797 (2014).
113. Alpert, D. J. & Hopke, P. K. A determination of the sources of airborne particles collected during the regional air pollution study. *Atmos. Environ.* **15**, 675–687 (1981).
114. Khedr, M. et al. Influence of New Year's fireworks on air quality—a case study from 2010 to 2021 in Augsburg, Germany. *Atmos. Pollut. Res.* **13** (2022).
115. Polissar, A. V., Hopke, P. K., Paatero, P., Malm, W. C. & Sisler, J. F. Atmospheric aerosol over Alaska: 2. Elemental composition and sources. *J. Geophys. Res.: Atmospheres* **D15**, 19045–19057 (1998).
116. Glojek, K. et al. Annual variation of source contributions to PM10 and oxidative potential in a mountainous area with traffic, biomass burning, cement-plant and biogenic influences. *Environ. Int.* 108787 (2024).
117. Brown, S. G., Eberly, S., Paatero, P. & Norris, G. A. Methods for estimating uncertainty in PMF solutions: examples with ambient air and water quality data and guidance on reporting PMF results. *Sci. Total Environ.* **518**, 626–635 (2015).
118. Pernigotti, D. & Belis, C. A. Deltasa tool for source apportionment benchmarking, description and sensitivity analysis. *Atmos. Environ.* **180**, 138–148 (2018).

## Acknowledgements

This study is funded by a grant from State Key Laboratory of Resources and Environmental Information System, the National Natural Science Foundation of China (42407566, 42205099). This study is also partly supported by the RI-URBANS project (Research Infrastructures Services Reinforcing Air Quality Monitoring Capacities in European Urban & Industrial Areas, European Union's Horizon 2020 research and innovation program, Green Deal, European Commission, contract 101036245). Meanwhile, samples in France were collected within many research and air quality assessment programs, including the programs CARA (funded by the Ministry of Environment, and coordinated by the LCSQA/Interis), DECOMBIO, CAMERA, and QAMECS (all the later ones funded by Ademe), QAMECS (funded by University Grenoble Alpes), OPE—Andra (funded by Andra), and multiple fundings by Atmo AuRA, Atmo Sud, Atmo Grand Est, Atmo Haut de France, Atmo Normandie, for the sampling and analyses. We would like to express our deep thanks to many people in the AASQA France for the sampling of all these samples, and to people in several laboratories in France, including IGE, for the analyses of these samples. The University of Aveiro acknowledges the financial support to CESAM by FCT/MCTES (UID Centro de Estudos do Ambiente e do Mar + LA/P/0094/2020). Vy Thuy Dinh PhD is funded by ANR ABS and grant Fondation UGA-UGA 2022-16 and grant PR-PRE-2021 FUGA-Foundation Air Liquide. IDAEA-CSIC was supported by the Ministry for Ecological Transition and Demographic Challenge of Spain and by Generalitat de Catalunya (D.G. Atmospheric Pollution Prevention and Control, and AGAUR 2017 SGR41), and by the Agencia Estatal de Investigación from the Spanish Ministry of Science and Innovation and, FEDER funds under the projects AIRPHONEMA (PID2022-142160OB-I00).

## Author contributions

Xiansheng Liu: Writing-original draft, Writing-review & editing, Conceptualization. Xun Zhang, Bowen Jin, Tao Wang: Methodology. Siyuan Qian, Jin Zou, Vy Ngoc Thuy Dinh, Jean-Luc Jaffrezo, Gaëlle Uzu, Pamela Dominutti, Sophie Darfeuil, Olivier Favez, Sébastien Conil, Nicolas Marchand, Sonia Castillo, Jesús D. de la Rosa, Stuart Grange, Konstantinos Eleftheriadis, Evangelia Diapouli, Manousos-Ioannis Manousakas, Maria Gini, Silvia Nava, Giulia Calzolari, Célia Alves, Cristina Reche: Data curation, review & editing. Roy M Harrison, Philip K. Hopke, Andrés Alastuey: Writing—

review & editing. Marta Monge: Project administration. Xavier Querol: Writing—review & editing, Supervision, Funding acquisition, Data curation.

## Competing interests

The authors declare no competing interests.

## Additional information

**Supplementary information** The online version contains supplementary material available at <https://doi.org/10.1038/s41612-025-01097-7>.

**Correspondence** and requests for materials should be addressed to Xun Zhang or Tao Wang.

**Reprints and permissions information** is available at <http://www.nature.com/reprints>

**Publisher's note** Springer Nature remains neutral with regard to jurisdictional claims in published maps and institutional affiliations.

**Open Access** This article is licensed under a Creative Commons Attribution-NonCommercial-NoDerivatives 4.0 International License, which permits any non-commercial use, sharing, distribution and reproduction in any medium or format, as long as you give appropriate credit to the original author(s) and the source, provide a link to the Creative Commons licence, and indicate if you modified the licensed material. You do not have permission under this licence to share adapted material derived from this article or parts of it. The images or other third party material in this article are included in the article's Creative Commons licence, unless indicated otherwise in a credit line to the material. If material is not included in the article's Creative Commons licence and your intended use is not permitted by statutory regulation or exceeds the permitted use, you will need to obtain permission directly from the copyright holder. To view a copy of this licence, visit <http://creativecommons.org/licenses/by-nc-nd/4.0/>.

© The Author(s) 2025

<sup>1</sup>Guangdong Key Laboratory of Environmental Catalysis and Health Risk Control, School of Environmental Science and Engineering, Guangdong-Hong Kong-Macao Joint Laboratory for Contaminants Exposure and Health, Institute of Environmental Health and Pollution Control, Guangdong University of Technology, 510006, Guangzhou, China. <sup>2</sup>Guangzhou Key Laboratory of Environmental Catalysis and Pollution Control, Guangdong Technology Research Center for Photocatalytic Technology Integration and Equipment Engineering, School of Environmental Science and Engineering, Guangdong University of Technology, 510006, Guangzhou, China. <sup>3</sup>Institute of Environmental Assessment and Water Research (IDAEA-CSIC), 08034 Barcelona, Spain. <sup>4</sup>School of Computer and Artificial Intelligence, Beijing Technology and Business University, 100048, Beijing, China. <sup>5</sup>Beijing Laboratory for System Engineering of Carbon Neutrality, Beijing Municipal Education Commission, 100048, Beijing, China. <sup>6</sup>School of Computer Science and Artificial Intelligence, Xinjiang HeTian College, 848000, Hotan, China. <sup>7</sup>Shanghai Key Laboratory of Atmospheric Particle Pollution and Prevention, Department of Environmental Science & Engineering, Fudan University, 200433, Shanghai, China. <sup>8</sup>Univ. Grenoble Alpes, IRD, CNRS, INRAE, Grenoble INP, IGE, UMR 5001, 38000 Grenoble, France. <sup>9</sup>INERIS, Parc Technologique Alata, BP 2, 60550 Verneuil-en-Halatte, France. <sup>10</sup>Laboratoire central de surveillance de la qualité de l'air (LCSQA), 60550 Verneuil-en-Halatte, France. <sup>11</sup>ANDRA DISTEC/EES Observatoire Pérenne de l'Environnement, F-55290 Bure, France. <sup>12</sup>Aix Marseille Univ, CNRS, LCE, Marseille, France. <sup>13</sup>Department of Applied Physics, University of Granada, 18011 Granada, Spain. <sup>14</sup>Andalusian Institute of Earth System Research, IISTA-CEAMA, University of Granada, 18006 Granada, Spain. <sup>15</sup>Associate Unit CSIC-UHU "Atmospheric Pollution," University of Huelva, 21071 Huelva, Spain. <sup>16</sup>Swiss Federal Laboratories for Materials Science and Technology (Empa), 8600 Dübendorf, Switzerland. <sup>17</sup>ENRAC Lab, National Centre for Scientific Research "Demokritos", Athens 15341, Greece. <sup>18</sup>INFN Division of Florence and Department of Physics and Astronomy, University of Florence, via G.Sansone 1, 50019 Sesto Fiorentino, Italy. <sup>19</sup>Department of Environment and Planning, Centre for Environmental and Marine Studies (CESAM), University of Aveiro, 3810-193 Aveiro, Portugal. <sup>20</sup>School of Geography Earth and Environmental Sciences, University of Birmingham, B15 2TT Birmingham, UK. <sup>21</sup>Departments of Public Health Sciences and Environmental Medicine, University of Rochester School of Medicine and Dentistry, Rochester, NY 14642, USA. <sup>22</sup>Institute for a Sustainable Environment, Clarkson University, Potsdam, NY 13699, USA. ✉e-mail: [zhangxun@btbu.edu.cn](mailto:zhangxun@btbu.edu.cn); [wangtao\\_fd@fudan.edu.cn](mailto:wangtao_fd@fudan.edu.cn)